Evaluation of Bleed Valve Rate Requirements in Nonlinear Control of Rotating Stall on Axial Flow Compressors *

Simon Yeung
cxy@indra.caltech.edu

Yong Wang
yongwang@indra.caltech.edu

Richard M. Murray
murray@indra.caltech.edu

Division of Engineering and Applied Science
California Institute of Technology
Pasadena, CA 91125

CDS Technical Report 98-001
17th February, 1998

Abstract

In this paper we evaluate the actuator rate requirements for control of rotating stall using a bleed valve and provide tools for predicting these requirements. Modification of both the stable and unstable parts of the compressor characteristic via addition of continuous air injection serves to reduce the requirement of a bleed valve used for the purpose of rotating stall stabilization. Analytical tools based on low order models (2-3 states) and simulation tools based on a reduced order model (37 states) are described. A bleed actuator rate limit study is presented to compare the actuator requirements predicted by theory, simulation, and experiment. The comparisons show that the predictions obtained from theory and simulations share the same trend as the experiments, with increasing accuracy as the complexity of the underlying model increases. Some insights on the design of a bleed-compressor pair are given.

Nomenclature

B, l_c, m, μ	compressor model parameters; see [12]
A	amplitude of first Fourier mode
A_{nom}	amplitude of first Fourier mode of fully developed stall cell
C_x	axial flow velocity
ϵ	noise level of the system expressed as a percentage of J
γ	throttle coefficient, $\Phi_T(\psi) = \gamma\sqrt{\psi}$
J	squared amplitude of first Fourier mode, $J = A^2$
K_{X}	gain estimation from method X
K_{RS}	gain for control of rotating stall in Liaw-Abed control law
K_{SU}	gain for control of surge in Eveker et al. [9] control law
R_{X}	rate estimation from method X
U	mean rotor speed
u	bleed valve control effort
u_{mag}	magnitude saturation of the bleed actuator as percentage of ϕ^*
u_{rate}	bleed valve rate limit in rotor revolutions for valve to open from fully closed

*Funding for this research was provided in part by AFOSR grant F49620-95-1-0409.

ρ	density of air
δP	pressure rise
ϕ	nondimensionalized axial flow velocity, $\phi = C_x/U$
ϕ^*	ϕ at peak of compressor characteristic
$\Phi_T(\psi)$	nondimensionalized throttle characteristic as a function of ψ
ψ	nondimensionalized pressure rise, $\psi = \delta P/(\rho U^2)$
ψ^*	ψ at peak of compressor characteristic
$\Psi_c(\phi)$	nondimensionalized compressor characteristic as a function of ϕ

1 Introduction

Rotating stall and surge are two types of instabilities that occur in axial flow compressor systems such as those in a gas turbine engine. Rotating stall refers to a non-axisymmetric flow perturbation that travels around the annulus of the compressor (sometimes referred to as a stall cell), while surge is a large axial oscillation of the flow. Typical effects of rotating stall and surge range from stress and wear on the compressor blades, to perturbation of the operation of the components downstream of the compressor in the engine, to destruction of the engine. Active control of rotating stall and surge can lead to an increase in the stability of a compressor against various disturbances such as inlet distortions and power transients. As a result, a compressor with active controls can operate closer to the current stall/surge line. The benefits can be realized in various ways including increased points of efficiency, lower take-off gross weight, lower specific fuel consumption, and stability/operability enhancement in maneuvers. Examples can be found in a set of reports prepared by Pratt and Whitney [15], General Electric Aircraft Engines [8], and Allison Gas Turbine [7] for the National Technical Information Service of the U.S. Department of Commerce on an evaluation of control concepts applied to gas turbine engine operations for both civilian and military aircraft.

Modeling and active control of rotating stall and surge has been investigated by a number of researchers. A simplified model was derived by Moore and Greitzer [12] for a compression system that exhibits rotating stall and surge. Based on this model, Liaw and Abed [16] derived a control law using a bleed valve for rotating stall. Experimental evaluations and analysis of other control laws using various types of actuators were investigated by other groups, including but not limited to Badmus et al. [1, 2], Paduano et al. [20], Day [6], Gysling et al. [13], D'Andrea et al. [5], Freeman et al. [10], Eveker et al. [9], and Yeung and Murray [24, 25]. Eveker et al. [9] is the first group to report successful experimental implementation of a bleed valve controller. In particular, the bleed valve actuation method tested by Eveker et al. [9] employs a 25 Hz (full open/full close) bleed valve and reports results on a compressor with a rotor frequency between 22.5 and 26.7 Hz; D'Andrea et al. [5] proposed a pulsed air injection method which uses 200 Hz binary injection actuators driven by solenoid valves on a compressor with a rotor frequency of 100 Hz; and the recirculation study reported in Freeman et al. [10] uses 300 Hz sleeve valves on a compressor with a 106 Hz stall frequency. For industrial applications where the compressors may be significantly more powerful (higher flow and pressure rise, higher rotor frequency, etc) than research compressors, obstacles such as control actuator magnitude and rate saturation can become crucial in these active control methods. Tools that predict and reduce the rate requirements of actuators for purposes of control of rotating stall in compressors can be valuable in designing actuators and circumventing possible actuator magnitude and rate limitations that may prevent successful active control implementations.

Attempts to control rotating stall on a single-stage, low-speed axial compressor at Caltech were carried out initially with a high speed bleed actuator and results were unsuccessful due to the fast growth rate of the stall cell relative to the rate limit of the valve [24]. It has been shown by D'Andrea

et al. [5] that air injection can be modeled as a shift of the compressor characteristic. By adding continuous air injection, the compressor characteristic is shifted favorably for bleed valve control of rotating stall and demonstration of control is achieved only with the compressor characteristic actuation [24, 25]. On the Caltech rig, the amount of compressor characteristic shifting can be varied by modifying the geometric features of the injection actuators setup [4], providing a family of compressor characteristics. In this paper, investigation of the trade-off between actuation of the compressor characteristic and the bleed valve rate requirement is carried out, with the following goals:

1. Identify possible functional dependence of the rate limit of a bleed valve in control of rotating stall on the shape of the compressor characteristic.

2. Provide a possible route to circumvent bleed valve rate limitation given the capability of actuation or modification of the compressor characteristic.

3. Provide insights for designing a compressor-bleed pair for purposes of stabilization of rotating stall.

This paper is organized as follows. Section 2 describes the features of a low order model of rotating stall and surge proposed by Moore and Greitzer [12]. The modeling of bleed actuation and continuous air injection is introduced as a modulation of the throttle [16] and compressor characteristic [5] respectively. The relevant control law will be given for the bleed valve. Analytical formulas are presented as theoretical tools used for predicting the minimum gain in the control law and rate limit of the bleed valve required for stabilization. A brief description of the simulation tools using a reduced order model proposed will end the section. Section 3 describes the experimental setup at Caltech including details of the sensing and actuation equipment. Section 4 presents the results of control of rotating stall using bleed valve with continuous air injection. A comparison study correlating the theory, simulation, and experiment in terms of the values of the gain and rate and the various features of the compressor characteristic is included to validate the theoretical and simulation tools. Finally, we summarize the findings of the investigation in Section 5.

2 Modeling and Theory

This section first gives a brief review of the main features of a low order model proposed by Moore and Greitzer [12]. Modeling of bleed actuation in the model is introduced and a review of a control law proposed by Liaw and Abed [16] is given. Expressions for the minimum gain and rate required for peak stabilization of rotating stall are presented. The section then ends with a brief description of the simulation tool using a high fidelity model proposed by Mansoux et al. [18].

2.1 Moore-Greitzer Model

To describe the basic behavior of the compression system, we make use of a low order model derived by Moore and Greitzer [12]. The model consists of three ordinary differential equations describing the evolution of the nondimensionalized axial flow velocity ϕ, nondimensionalized pressure rise ψ,

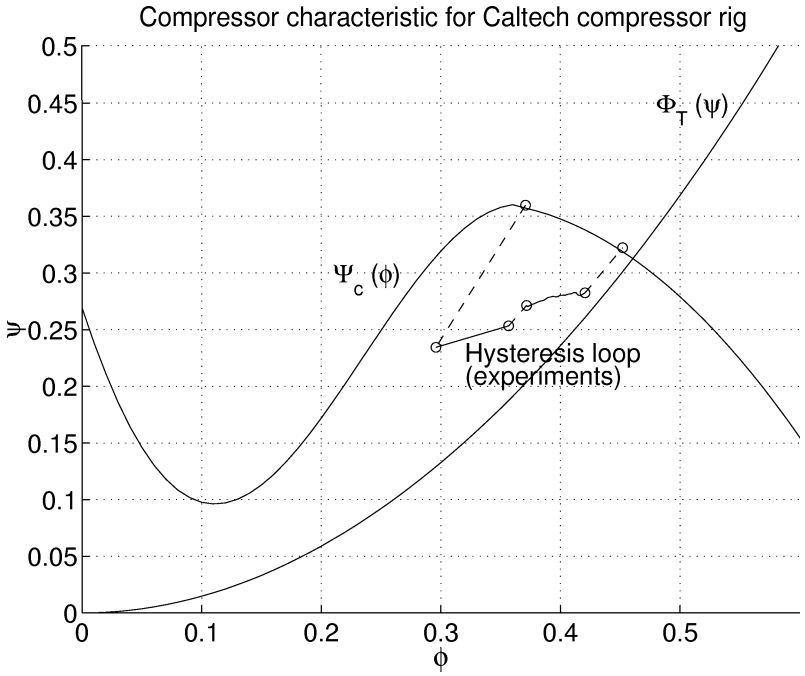

Figure 1: Typical compressor characteristic and stalled operation

and the square of the amplitude of the first Fourier mode $J = A^2$:

$$\begin{aligned}
\dot{\psi} &= \frac{1}{4l_cB^2}(\phi - \Phi_T(\psi)), \\
\dot{\phi} &= \frac{1}{l_c}(\Psi_c(\phi) - \psi + \frac{J}{4}\frac{\partial^2\Psi_c(\phi)}{\partial\phi^2}), \\
\dot{J} &= \frac{2}{\mu+m}J(\frac{\partial\Psi_c(\phi)}{\partial\phi} + \frac{J}{8}\frac{\partial^3\Psi_c(\phi)}{\partial\phi^3}),
\end{aligned} \tag{1}$$

where the throttle characteristic $\Phi_T(\psi) = \gamma\sqrt{\psi}$ with γ being the throttle coefficient. The compressor characteristic $\Psi_c(\phi)$ is a map containing information about the performance of the compressor at various values of the flow in the system. Figure 1 shows an example of a compressor characteristic and a hysteresis loop associated with rotating stall obtained experimentally.

The equilibria of the system are stable for large values of the throttle coefficient γ. As γ is decreased, a critical value γ^* is reached and the system exhibits a subcritical transcritical bifurcation in the J-γ plane (Figure 2). Since $J = A^2 \geq 0$, we ignore the negative branch of the bifurcation diagram for rotating stall. At $\gamma = \gamma^*$, the stability of the $J = 0$ equilibrium point changes from stable to unstable. However, there is a stable $J > 0$ equilibrium that coexists with the $J = 0$ equilibrium, and thus the system stalls. With $J > 0$, if the value of γ is increased, the system continues to stay along the $J > 0$ branch of solution instead of unstalling immediately. The system eventually unstalls when the value of γ reaches a point where the $J > 0$ solution loses stability. This behavior is observed on axial compressors as a hysteresis loop due to rotating stall.

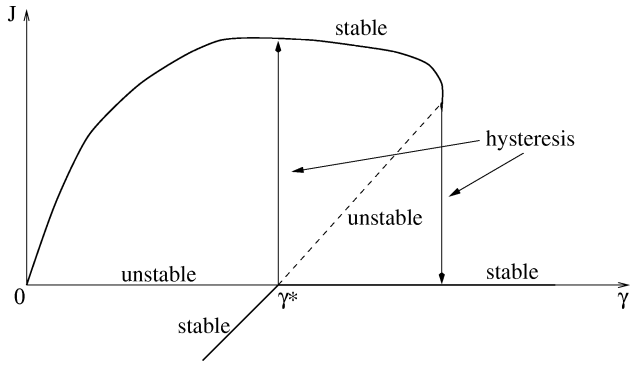

Figure 2: Transcritical bifurcation in J-γ plane.

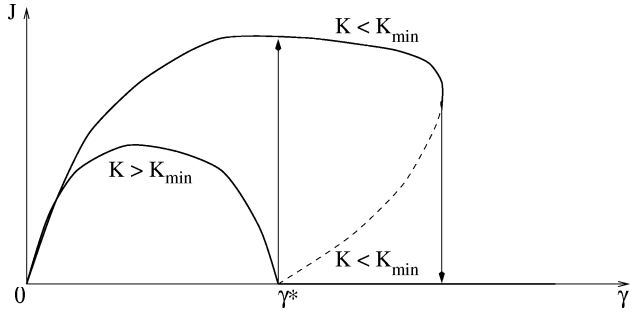

Figure 3: Relation of controller gain and behavior of bifurcation.

2.2 Bleed Valve Control

For stall control, Liaw and Abed [16] proposed a control law that modifies the throttle characteristic:

$$\begin{aligned} \Phi_T(\psi) &= (\gamma + u)\sqrt{\psi}, \\ u &= K_{\mathrm{RS}} J. \end{aligned}$$

This control law can be realized experimentally through the use of a bleed valve. For a large enough value of K_{RS}, the nominally unstable branch of equilibrium solution created at $\gamma = \gamma^*$ "bends over" and eliminates the hysteresis loop, i.e. the subcritical nature of the transcritical bifurcation is changed to supercritical (Figure 3).

By substituting the stall control law and computing the quantity $\frac{dJ}{d\gamma}$ at the stall inception throttle coefficient γ^*, the minimum gain needed for this phenomenon to occur can be found by asserting the condition that $\frac{dJ}{d\gamma}|_{\gamma=\gamma^*} < 0$ (see Figure 3). The expression for the minimum gain required for peak stabilization is given by

$$K_{\mathrm{theory}} = K_{\mathrm{RS,min}} = -\frac{\phi^* \Psi_c'''(\phi^*)}{8\gamma^* \psi^* \Psi_c''(\phi^*)} - \frac{\gamma^* \Psi_c''(\phi^*)}{8\psi^*}, \tag{2}$$

which depends on the shape of the compressor characteristic. Since the second term is always non-negative around the peak, the larger the value of $\Psi_c'''(\phi^*)$ the smaller $K_{\mathrm{RS,min}}$. Roughly speaking, this amounts to a compressor characteristic which is more "filled out" to the left of the peak. This expression serves as one of the theoretical tools for predicting the bleed valve requirement needed for peak stabilization.

In addition to the minimum gain, the requirement on the characteristics of the bleed actuator for control of stall can also be analyzed. The detailed theoretical analysis for the effects of actuator

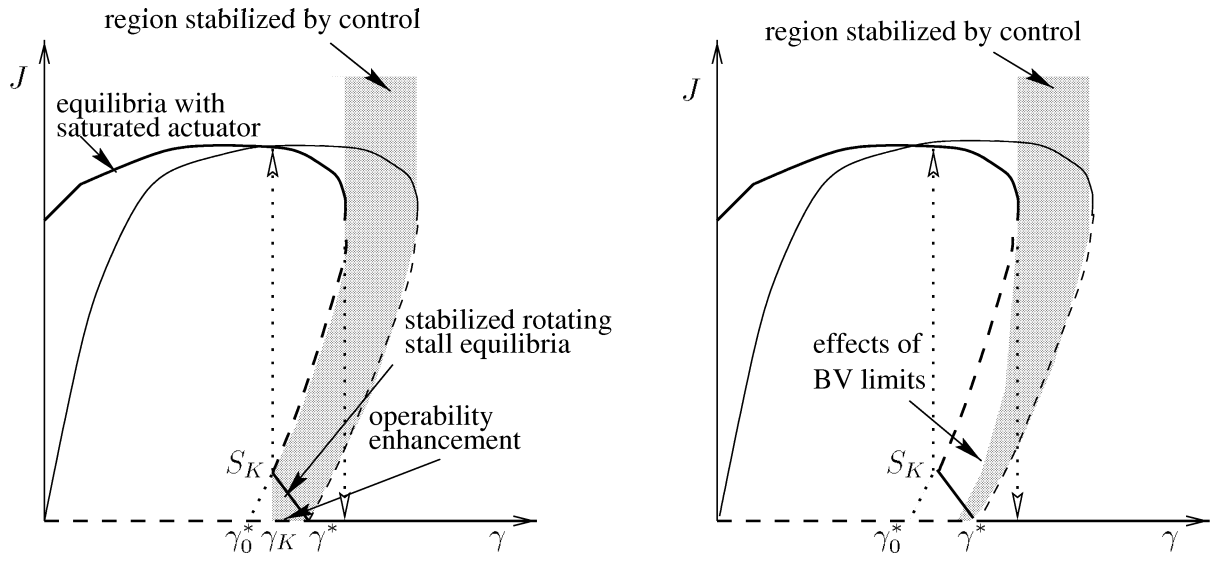

(a) Saturation with infinite bandwidth

(b) Saturation with finite bandwidth

Figure 4: Effects of Liaw-Abed control law with actuator limits. Solid line: stable equilibria, dashed line: unstable equilibria.

limits can be found in Wang and Murray [21]. In the following we only sketch the ideas qualitatively and present the main results that are used for comparisons in later sections.

A study of the effects of actuator magnitude and rate saturations can be motivated using Figure 4. Figure 4(a) shows the effects of the Liaw-Abed controller with finite magnitude saturation and infinite bandwidth. The bleed valve controller fails to stabilize stall when the magnitude saturation is reached, and thus cannot eliminate the hysteresis loop beyond γ_K. Furthermore, any arbitrarily small noise of J will grow to fully developed rotating stall no matter how big the controller gain is if the throttle is operated at $\gamma < \gamma_0^*$. It can also be seen that the region that benefits from the controller is much smaller than the unsaturated case (Figure 3) if the magnitude saturation is severe.

Suppose now that the rate limit is finite in addition to the magnitude saturation. Then the region that benefits from the bleed valve control is even smaller (shaded region in Figure 4(b)). Roughly speaking, the region of attraction of the operable equilibria is decreased as the rate limit of the actuator decreases. As a result the extended operable region is further restrained.

The noise level for a real compression system is not arbitrarily small. When the noise level is of finite amplitude, the open loop system will go to rotating stall at a throttle coefficient which is larger than γ^*. In this case, region benefited from active control becomes even smaller. In the following we give an approximate analysis to evaluate the shaded region in Figure 4.

Consider the Moore-Greitzer model given in equation (1). Suppose the Greitzer B parameter is sufficiently small, such that the surge dynamics is exponentially stable, and the compressor characteristic is smooth. The transcritical bifurcation for the uncontrolled system at γ^* implies the existence of a center manifold near the transcritical bifurcation point. By viewing the control input u as a parameter, system (1) can be reduced to the center manifold when the throttle is operated near the stall inception point γ^*. The dynamics on the center manifold is given by the following one dimensional system

$$\dot{J} = \alpha_1(\delta + u)J + \alpha_2 J^2, \tag{3}$$

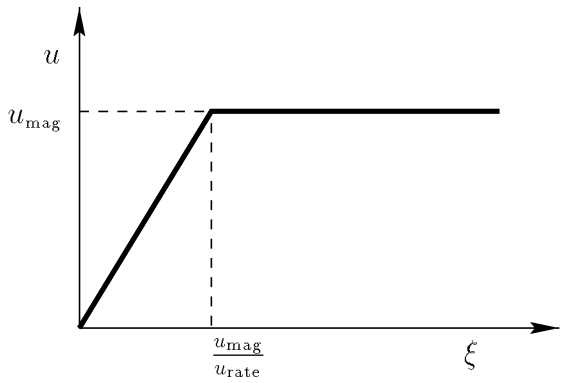

Figure 5: Controllers constrained by magnitude and rate limits

where

$$\begin{aligned}\delta &= \gamma - \gamma^*,\\ \alpha_1 &= \frac{2\sqrt{\psi^*}\Psi_c''}{m+\mu},\\ \alpha_2 &= \frac{1}{4(m+\mu)}\left(\Psi_c''' + \frac{\gamma^*\Psi_c''^2}{\sqrt{\psi^*}}\right),\end{aligned}$$

and all the derivatives are evaluated at the peak of the compressor characteristic. To account for the magnitude and rate limits of the control input u, we assume that the actuator opens according to the rate limit and saturates (see Figure 5). The system then has the following boundary conditions.

$$\begin{aligned} J(0) &= \epsilon, & u(0) &= 0,\\ J(\tfrac{u_{\mathrm{mag}}}{u_{\mathrm{rate}}}) &= J_c = -\frac{\alpha_1}{\alpha_2}(u_{\mathrm{mag}}+\delta), & u(\tfrac{u_{\mathrm{mag}}}{u_{\mathrm{rate}}}) &= u_{\mathrm{mag}}, \end{aligned} \tag{4}$$

where ϵ is the noise level of the system.

The analytical solution to equation (3) can be difficult to obtain. However, an approximation to the solution of this two-point boundary value system can be obtained. The rate limit requirement for stall stabilization in a system of a given noise level can then be found [21]. Let

$$\begin{aligned} \Delta &= 1 + \frac{\alpha_1\delta}{\alpha_2\epsilon}, & \eta &= \alpha_2\epsilon\xi, & f &= \frac{J}{\epsilon}, & J_c &= \epsilon(\sigma+1-\Delta),\\ \sigma &= \frac{-\alpha_1 u_{\mathrm{mag}}}{\alpha_2\epsilon}, & \bar{\eta} &= \alpha_2\epsilon\tfrac{u_{\mathrm{mag}}}{u_{\mathrm{rate}}}, & f' &= \frac{df}{d\eta}, & \lambda &= \frac{\sigma}{\bar{\eta}}, \end{aligned}$$

then equation (3) with initial and final conditions (4) can be written as follows:

$$\begin{aligned} f' &= (\Delta - 1 - \lambda\eta)f + f^2,\\ f(0) &= 1,\\ f(\bar{\eta}) &= 1 + \sigma - \Delta. \end{aligned}$$

The approximation to the solution of $f(\bar{\eta})$ can be obtained as follows. Additional boundary conditions characterizing derivatives at the boundaries can be obtained from f'. A form for the function f is then assumed while satisfying the desired boundary conditions. For instance, by letting $f(\eta)$ satisfy the following boundary conditions,

$$f(0) = 1, \quad f(\bar{\eta}) = 1 + \sigma - \Delta, \quad f'(0) = \Delta, \quad f'(\bar{\eta}) = 0.$$

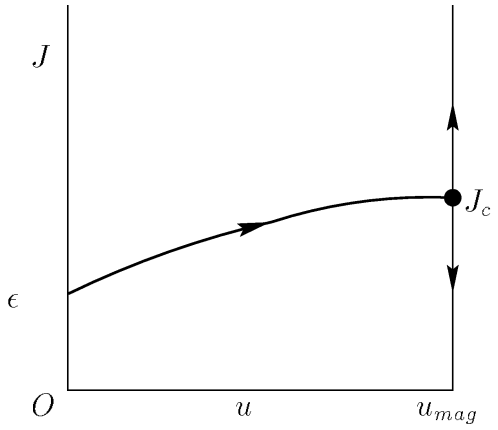

Figure 6: The phase portrait of the system (equation (3)).

we obtain

$$R1_{\text{theory}} = \frac{u_{\text{mag}}}{1 + \frac{\pi}{8}\sigma\bar{\eta}^2 \arctan\left(\frac{\pi}{4}\sigma\bar{\eta}\right)} \tag{5}$$

after algebraic manipulations. Alternatively,

$$R2_{\text{theory}} = u_{\text{mag}} \frac{1 - \frac{2}{\pi}\arctan\left(\frac{\pi}{4}\sigma\bar{\eta}\right)}{1 - \frac{\sigma}{1+\sigma}\frac{2}{\pi}\arctan\left(\frac{\pi}{4}\sigma\bar{\eta}\right)} \tag{6}$$

is obtained if a slightly different set of boundary conditions is chosen (see Wang and Murray [21] for details). These different boundary conditions essentially translate to different values of the growth/decay as the trajectory of J starts and ends (see Figure 6).

Formulas (5) and (6) are used in later sections of this paper to compare with results from simulations of a high fidelity model and experiments.

2.3 Simulation Model

A high fidelity model proposed by Mansoux et al. [18] is used as the basis of the simulation tool. The model proposed by Mansoux et al. [18] takes the form

$$\begin{aligned} \dot{\phi} &= -\tilde{E}^{-1} \cdot \tilde{A} \cdot \phi + \Psi_c(\phi) - T \cdot \bar{\psi}, \\ \dot{\bar{\psi}} &= \frac{1}{4B^2 l_c}(S \cdot \phi - \Phi_T(\bar{\psi})), \end{aligned}$$

where

$$\begin{aligned} \tilde{E} &= G^{-1} \cdot D_E \cdot G, \\ \tilde{A} &= G^{-1} \cdot D_A \cdot G, \\ D_E &= \begin{bmatrix} l_c & 0 & 0 & 0 & \dots & 0 \\ 0 & (\frac{m}{1} + \mu) & 0 & 0 & \dots & 0 \\ 0 & 0 & (\frac{m}{1} + \mu) & 0 & \dots & 0 \\ & & \vdots & & & \\ 0 & 0 & 0 & \dots & (\frac{m}{N} + \mu) & 0 \\ 0 & 0 & 0 & \dots & 0 & (\frac{m}{N} + \mu) \end{bmatrix}, \end{aligned}$$

$$
\begin{aligned}
D_A &= \begin{bmatrix} 0 & 0 & 0 & 0 & \dots & 0 \\ 0 & 0 & \lambda & 0 & \dots & 0 \\ 0 & -\lambda & 0 & 0 & \dots & 0 \\ & & \vdots & & & \\ 0 & 0 & 0 & \dots & 0 & N\lambda \\ 0 & 0 & 0 & \dots & -N\lambda & 0 \end{bmatrix}, \\
G &= \sqrt{\frac{2}{M}} \begin{bmatrix} \frac{1}{\sqrt{2}} & \frac{1}{\sqrt{2}} & \dots & \frac{1}{\sqrt{2}} \\ \cos(\theta_1) & \cos(\theta_2) & \dots & \cos(\theta_M) \\ \sin(\theta_1) & \sin(\theta_2) & \dots & \sin(\theta_M) \\ \cos(2\theta_1) & \cos(2\theta_2) & \dots & \cos(\theta_M) \\ \sin(2\theta_1) & \sin(2\theta_2) & \dots & \sin(2\theta_M) \\ \vdots & \vdots & \vdots & \vdots \\ \cos(2\theta_1) & \cos(2\theta_2) & \dots & \cos(\theta_M) \\ \sin(N\theta_1) & \sin(N\theta_2) & \dots & \sin(N\theta_M) \end{bmatrix}, \\
\theta_n &= \frac{2\pi n}{M}, \\
S &= \begin{bmatrix} \frac{1}{M} & \frac{1}{M} & \dots & \frac{1}{M} \end{bmatrix}, \\
T &= \begin{bmatrix} 1 & 1 & \dots & 1 \end{bmatrix}^{\mathrm{T}},
\end{aligned}
$$

and $M = 2N+1$, where N is the number of Fourier modes. This formulation of the Moore-Greitzer model [12] is suitable for control analysis and design, and allows accounting of higher modes.

Some realistic considerations are included. One example of such effects is unsteady losses [14] with the form:

$$
\begin{aligned}
\Psi_c = \Psi_{c,\mathrm{qs}} &= \Psi_{c,\mathrm{isen}} - L_r - L_s, \\
\dot{L_r} &= \frac{1}{\tau_r}(L_{r,\mathrm{ss}} - L_r), \\
L_{r,\mathrm{ss}} &= R(\Psi_{c,\mathrm{isen}} - \Psi_{c,\mathrm{qs}}), \\
\dot{L_s} &= \frac{1}{\tau_s}(L_{s,\mathrm{ss}} - L_s), \\
L_{s,\mathrm{ss}} &= (1-R)(\Psi_{c,\mathrm{isen}} - \Psi_{c,\mathrm{qs}}),
\end{aligned}
$$

where $\Psi_{c,\mathrm{qs}} = \Psi_c$ denotes the quasi-static compressor characteristic, $\Psi_{c,\mathrm{isen}}$ the isentropic compressor characteristic, L_r the losses associated with the rotor, L_s the losses associated with the stator, R the reaction, and subscript ss steady-state. Another example is the dynamics of the actuator such as magnitude, bandwidth, and rate limitations. For the simulations reported in this paper, a simulation with five Fourier modes resulting in 34 states for the compressor, and 3 states for the bleed actuator is used.

3 Experimental Setup

The Caltech compressor rig is a single-stage, low-speed, axial flow compressor with sensing and actuation capabilities. Figure 7 shows a drawing of the rig and Figure 8 a magnified view of the sensor and injection actuator ring.

The compressor is an Able Corporation model 29680 low speed single stage axial compressor with 14 blades, a tip radius of 8.5 cm, and a hub radius of 6 cm. The blade stagger angle varies

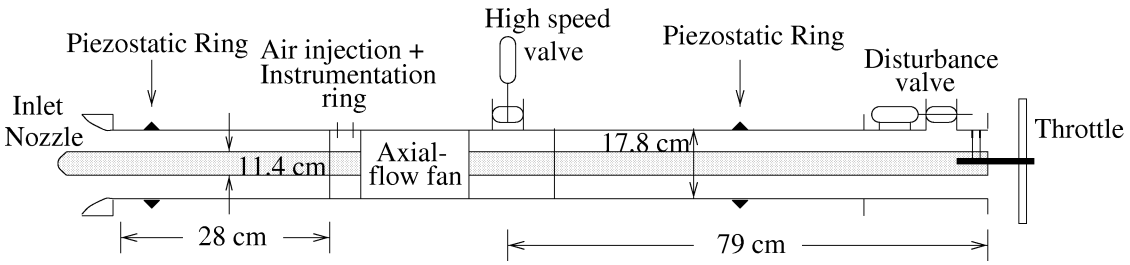

Figure 7: Experimental setup.

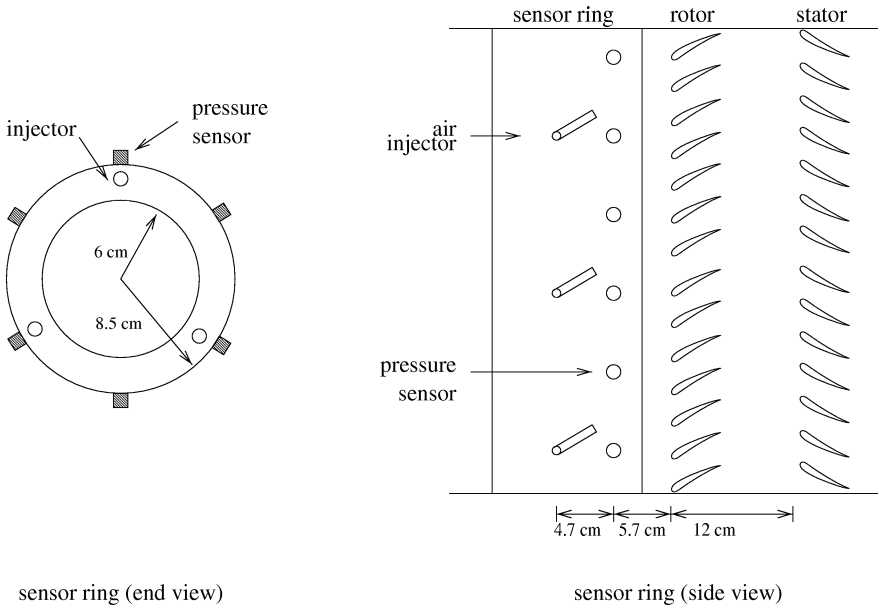

Figure 8: Sensor and injection actuator ring.

from 30° at the tip to 51.6° at the hub, and the rotor to stator distance is approximately 12 cm (1.4 rotor radii). Experiments are run with a rotor frequency of 100 Hz, giving a tip Mach number of 0.17. In the configuration shown in Figure 7, rotating stall is observed to occur with a frequency of approximately 67 Hz. With a plenum attached at the outlet (for compliance effects), surge occurs at approximately 1.8 Hz. Data taken for a stall transition event suggests that the stall cell grows from the noise level to its fully developed size in approximately 30 msec (3 rotor revolutions). At the stall inception point, the velocity of the flow through the compressor is approximately 16 m/sec.

Six static pressure transducers with 1000 Hz bandwidth are evenly distributed along the annulus of the compressor at approximately 5.7 cm (1.1 rotor radii) from the rotor face. By performing a discrete Fourier transform on the signals from the transducers, the amplitude and phase of the first and second Fourier modes of the pressure perturbation of a nonaxisymmetric disturbance can be obtained. The difference between the pressure obtained from one static pressure transducer mounted at the piezostatic ring at the inlet and that from the piezostatic ring downstream near the outlet of the system is computed as the pressure rise across the compressor. For the velocity of the system, a hotwire anemometer is mounted approximately 13.4 cm (1.6 rotor radii) upstream of the rotor face. All of the sensor signals are filtered through a 4th order Bessel low pass filter with a cutoff frequency of 1000 Hz before the signal processing phase in the software.

A high speed and a low speed bleed valve are available on the Caltech rig. The high speed

bleed valve, used primarily for stall control, has a magnitude saturation of 12% (corresponding to an area of 11.4 cm^2) of the flow at the stall inception point and is approximately 26 cm (3.1 rotor radii) downstream of the rotor. The low speed valve, used primarily for surge control and throttle disturbance generation, has a magnitude saturation of 30% of the flow of the system at the stall inception point and is estimated to have a small signal ($\pm 5°$ angle modulation) bandwidth of 50 Hz and a large signal ($\pm 90°$ angle modulation) bandwidth of 15 Hz.

The air injectors are on-off type injectors driven by solenoid valves. For applications on the Caltech compressor rig, the injectors are fed with a pressure source supplying air at a maximum pressure of 80 psig. The injectors are located at approximately 10.4 cm (1.2 rotor radii) upstream of the rotor. Due to significant losses across the solenoid valves and between the valves and the pressure source, the injector back pressure reading does not represent an accurate indication of the actual velocity of the injected air on the rotor face. Using a hotwire anemometer, the maximum velocity of the velocity profile produced by the injected air measured at a distance equivalent to the rotor-injector distance for 50 and 60 psig injector back pressure are measured to be approximately 30.2 and 33.8 m/sec respectively. At the stall inception point, each injector can add approximately 1.7% mass, 2.4% momentum, and 1.3% energy to the system when turned on continuously at 60 psig injector back pressure. The bandwidth associated with the injectors is approximately 200 Hz at 50% duty cycle. The angle of injection, injector back pressure, the axial location of the injectors, and the radial location of the injectors can all be varied.

All experiments are run in real time using Sparrow [19] with a sampling frequency of 2000 Hz on a Pentium 100 MHz PC.

4 Results

In this section, we present the results for axisymmetric bleed with continuous air injection. Control of rotating stall is demonstrated first. A description of the procedure leading to the comparison study is then given, followed by the results.

4.1 Demonstration of Control

At certain injector angles and locations, different injector back pressure can reduce the size of the open-loop hysteresis loop by different amounts on the Caltech rig. Addition of continuous air injection is conjectured to reduce rate and magnitude requirements for bleed valve controls of rotating stall by changing the compressor characteristic.

To validate the conjecture, the air injector angle is set at 27° (with positive angles implying counter-compressor-rotation) and 60 psig injector back pressure. With the plenum attached, surge cycle data is taken and the algorithm for identifying the unstable part of the compressor characteristic as described by Behnken [3]. Figure 9 shows the results.

The identified compressor characteristic is more "filled out" on the left of the peak. The crosses in Figure 9 are experimental data points of the stable side of the compressor characteristic with continuous air injection, the right solid curve the polynomial fit of the experimental data points, the left solid curve the identified unstable part of the characteristic in the presence of continuous air injection, the dashed the compressor characteristic with no air injection, and the shaded region the experimental surge cycles data for $\Psi_c(\phi)$ in the presence of air injection. As shown in the figure, the shape of the compressor characteristic is shifted in the presence of continuous air injection.

The shifting of the compressor characteristic serves to reduce the bandwidth and rate requirement of the bleed valve for control of rotating stall. To observe this phenomenon, equation (2) can serve as an initial tool. Equation (2) gives a formula to the minimum gain required for stabilization

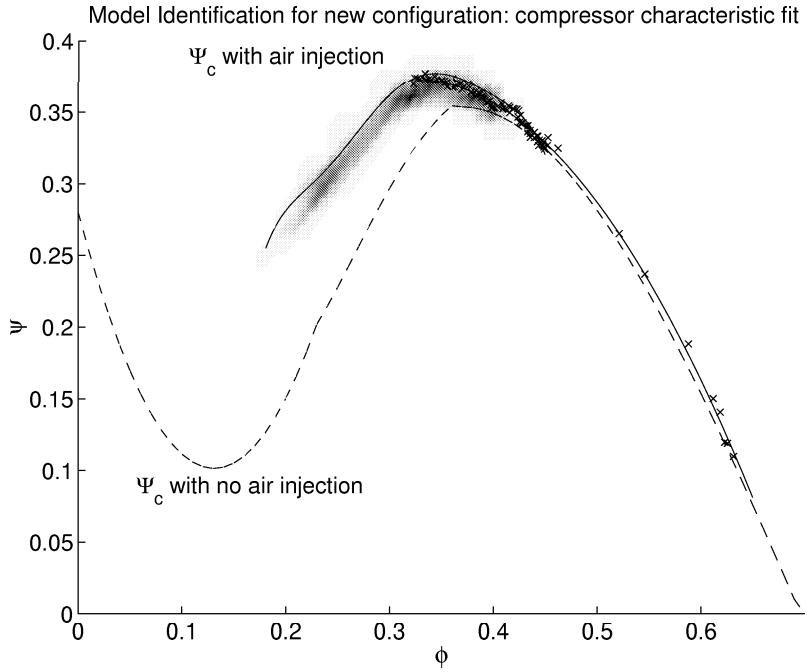

Figure 9: Identification of compressor characteristic with continuous air injection at 27° and 60 psig injector back pressure. The crosses represent data points taken from experiments, the solid the identified compressor characteristic, the dashed the compressor characteristic without air injection, and the shaded region the experimental surge cycles data for $\Psi_c(\phi)$ with air injection.

of rotating stall at the peak of the compressor characteristic. A 4th order polynomial fit to the unactuated compressor characteristic in Figure 9 gives

$$\Psi_c(\phi) = 0.71 - 10.59\phi + 60.80\phi^2 - 126.39\phi^3 + 87.48\phi^4,$$

with the peak at $(\phi, \psi) = (0.38, 0.35)$, and the second and third derivative values of -14.99 and 39.45 respectively. A similar fit to the actuated characteristic gives

$$\Psi_c(\phi) = 0.78 - 8.82\phi + 49.49\phi^2 - 104.77\phi^3 + 74.1331\phi^4,$$

with the peak at $(\phi, \psi) = (0.35, 0.38)$, and the second and third derivative values of -12.07 and -5.92 respectively. Equation (2) applied to the unactuated characteristic gives $K_{\mathrm{RS,min,unact}} = 4.00$ and to the actuated case gives $K_{\mathrm{RS,min,act}} = 2.16 < K_{\mathrm{RS,min,unact}}$.

With this evidence, a detailed experiment is carried out with the injector back pressure set at 55 psig. Figure 10 shows the open- and closed-loop behavior of the system in the ϕ-ψ plane and the γ-J plane respectively.

The closed-loop behavior shows no hysteresis loop on Figure 10, as expected from the theory. As Figure 10 shows, after the bleed valve saturates, the system returns to the original stalled equilibria. The γ-J plot in Figure 10 is expected to show the same observation. The mismatch at low values of γ is due to the formation of the second mode of stall in the open-loop case. For the open-loop system with continuous air injection, the second mode of rotating stall forms at a value of γ smaller than that for the formation of the first mode. At $\gamma = 0.45$ on Figure 10, the second mode forms and becomes dominant, and the amplitude of the first mode is decreased. Further decrease in γ leads to a further reduction in the amplitude of the first mode. At around $\gamma = 0.33$, the throttle

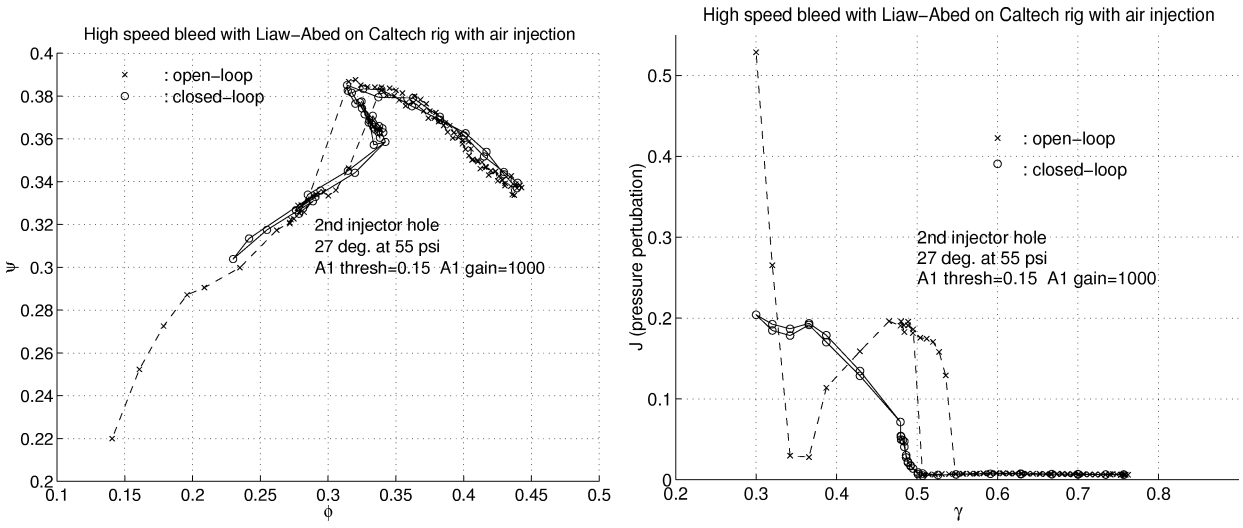

Figure 10: Open- and closed-loop behavior of system on ϕ-ψ plane for control with bleed valve and continuous air injection at 55 psig injector back pressure.

is almost fully closed and the first mode becomes dominant again. In the closed-loop case, this phenomenon is not observed since the high speed bleed valve saturates and remains open. As a result, the main flow level is not low enough for the second mode of rotating stall to form.

4.2 Procedure for Comparison Study

We now compare the rate predictions derived in Section 2 with the experimental results. The air injectors back pressure and angle are varied to produce a set of scenarios. Data is taken and analyzed to obtain the theoretical and simulation predictions, as well as the experimental values for the rate limit requirement for stabilization of stall.

The amount of the effects of air injection on the system can be varied by modifying various geometrical characteristics of the injector location and configuration [4]. For this study, the injector angle relative to the axial flow direction is varied between 27° and 40° in the opposite direction of the rotor rotation, and the back pressure of the injectors is varied between 40 to 60 psig, producing a total of 16 different scenarios and the nominal open-loop system without air injection. At the various injection settings, experiments are carried out to obtain the gain and rate values required for peak stabilization. For this study, peak stabilization is achieved if the following conditions are met during the experiment:

$$\begin{aligned} \phi &\geq 0.9\phi^*, \\ A &\leq 0.5A_{\text{nom}}, \end{aligned}$$

where ϕ is the axial velocity and A is the amplitude of the first Fourier mode, ϕ^* is the flow at stall inception, and A_{nom} is the amplitude of fully developed stall without bleed valve control. It should be noted that ϕ^* is taken experimentally at the stall inception point for each of the case of the injection setting under consideration.

The rate limits are determined on the experiment as follows. A function is written to increment the gain until the conditions of peak stabilization are met. An analogous function is written for the rate. The gain/rate required for peak stabilization is then obtained by first setting the system operating point to stable but near stall inception. With the rate/gain fixed, injection and the

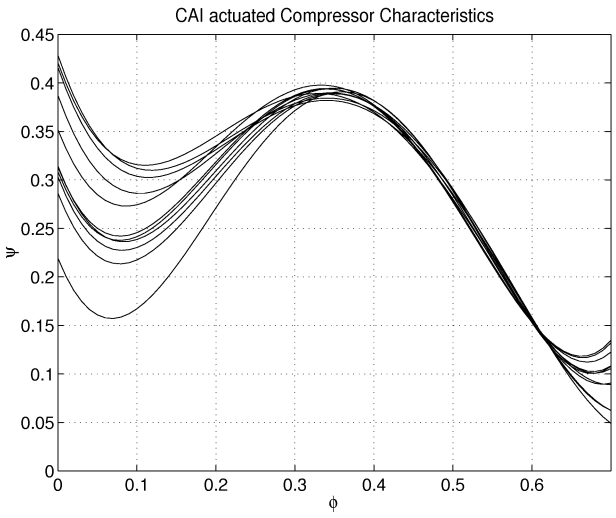

Figure 11: Fitted compressor characteristics for the 11 cases.

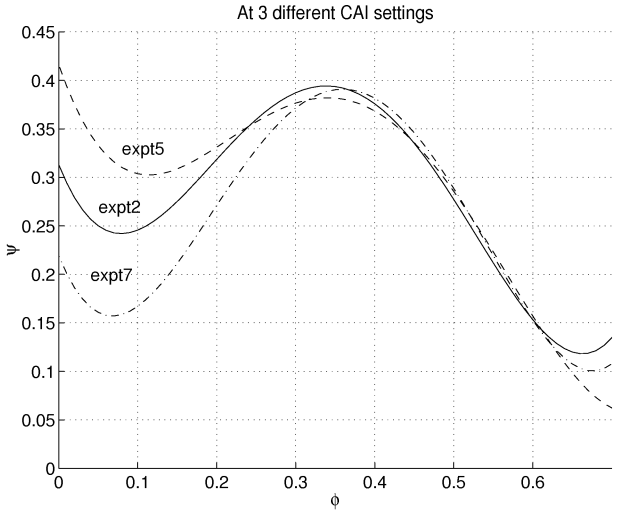

Figure 12: Identified compressor characteristics at 3 different continuous air injection settings.

controller is then activated with the gain/rate set to zero. The load of the compressor is then increased by changing the throttle setting until a nominally unstable operating point is reached. The gain/rate incrementing function then increments the variable of interest until peak stabilization is achieved. The gain and rate obtained from the experiments are referred to as K_{expt} and R_{expt} respectively.

Among the 17 injection settings, peak stabilization is achieved in 11 cases and the nominally stable side of the compressor characteristic is experimentally recorded at each of the 11 settings. The unstable sides for each of these cases are identified by using surge cycle data with an algorithm proposed by Behnken [3]. For this study, a fourth order polynomial is used to approximate the piecewise continuous curve for each case. Figure 11 shows the fitted compressor characteristics. These polynomial compressor characteristics are then used with realistic values of various parameters (e.g. noise level in system) in analytical relations K_{theory}, $R1_{\text{theory}}$, and $R2_{\text{theory}}$, and in simulations that estimate the gain K_{simu} and rate R_{simu} requirements on the bleed valve for stall stabilization.

There is uncertainty associated with the computation of the theoretical predictions and the experimental data. Due mainly to the unsteadiness of the fluid in the system, there is uncertainty in each of the identified compressor characteristics from the 17 settings. Results computed using these characteristics thus inherit the uncertainty which needs to be accounted for. The experiment gain and rate data also has uncertainty associated with it again due primarily to unsteadiness of the system.

To determine the level of uncertainty associated with the theoretical predictions and the experiments, an investigation is carried out on 3 of the 11 points, namely, experiment number 2 (expt2), 5 (expt5), and 7 (expt7) (see Figure 12). For each of these settings, ten different segments of the surge cycle data are used to identify the unstable side of the compressor characteristic. The resulting characteristics are then used to compute the theoretical predictions, and 95% confidence error bars (adjusted with T-statistics) are obtained for K_{theory}, $R1_{\text{theory}}$, and $R2_{\text{theory}}$. Similarly, for the uncertainty associated with the experimental gain and rate data, ten experiments are carried out for expt2, expt5, and expt7, to give 95% confidence error bars on K_{expt} and R_{expt}.

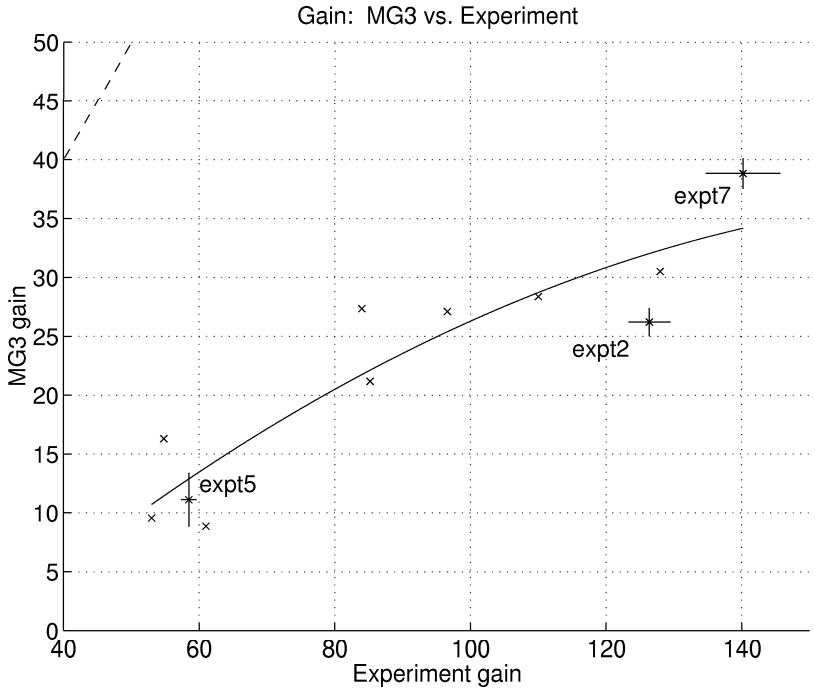

Figure 13: Comparison of gain predicted by MG3 and experimental gain required for stabilization of stall. The bars in the x direction are error bars associated with the the uncertainty in computing the theoretical gain values (through identifying the unstable of $\Psi_c(\phi)$ using surge cycle data); the bars in the y direction are error bars associated with the experimentally obtained values.

4.3 Comparison Study

Based on the functional dependence of the analytical relations for the minimum gain and rate requirement on $\Psi_c''(\phi^*)$ and $\Psi_c'''(\phi^*)$, an examination of Figure 12 would indicate that experiment 5 should require the least gain/rate while experiment 7 should require the most. The theory and simulations are expected to show at least a qualitative trend with respect to the experiment.

The values of the gain predicted by the theory are plotted against the gains obtained on the experiments in Figure 13. In all of the plots presented in this section, the dashed line represents the one-to-one line between the theoretically and experimentally obtained values. As shown in the figure, the K_{theory} estimates are not quantitatively reliable but do present the qualitative monotonic trend as expected. The main factor contributing to the quantitative disagreement between K_{theory} and the experiment is the lack of actuator dynamics in the derivation of the analytical expression. The bleed valve is assumed to be ideal with infinite bandwidth and magnitude saturation in the analysis while actuator limits are present in the experiments. Nevertheless, experiment 5 is predicted and verified to require the least gain, and experiment 7 the most.

The values of the rate predicted by the two analytical relations, $R1_{\text{theory}}$ and $R2_{\text{theory}}$ are plotted against the rates obtained on the experiments in Figure 14. First of all, it should be pointed out that the experiments show that the rate requirement for peak stabilization is reduced from approximately 3300 cm^2/sec to below 230 cm^2/sec (with a magnitude saturation at 11.4 cm^2) by varying the amount of compressor characteristic actuation. Regarding the theoretical tools used for prediction, one can see from the figure that $R1_{\text{theory}}$ predicts the rate requirement more accurately than $R2_{\text{theory}}$. Furthermore, $R1_{\text{theory}}$ seems to be more accurate at more severe rate limit values. The main difference between the two expressions originates from the different ways an approximation

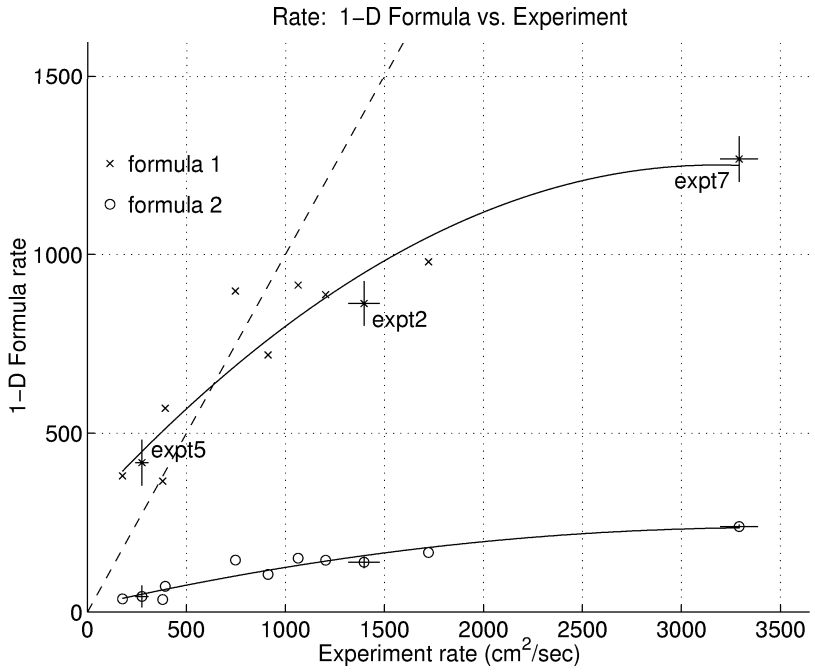

Figure 14: Comparison of rate predicted by theory and experimental rate required for stabilization of stall. The bars in the x direction are error bars associated with the uncertainty in computing the theoretical rate values (through identifying the unstable of $\Psi_c(\phi)$ using surge cycle data), and the bars in the y direction the error bars associated with the experimentally obtained values.

to the solution to the one-dimensional center manifold (eq. (3)) of the Moore-Greitzer equations is made. Despite their quantitative differences, a monotonic trend similar to that observed in the theoretical gain comparison is again displayed.

The values of gain and rate predicted by simulations are plotted against the experimental values in Figure 15. The gain and rate estimates of the simulations match with the experimentally obtained counterpart more closely than the theoretical predictions. However, there are a number of factors affecting the remaining difference. A possible explanation for this phenomenon is that the only difference in the 11 simulations are the compressor characteristics and the effective length parameter in the model l_c. The effects of continuous air injection on the system in certain cases may require modifying more parameters in order to accurate capture the reality. A more careful identification of the system at each point should present a more reliable simulation.

From the K_{theory} expression,

$$K_{\text{theory}} = -\frac{\phi^* \Psi_c'''(\phi^*)}{8\gamma^* \psi^* \Psi_c''(\phi^*)} - \frac{\gamma^* \Psi_c''(\phi^*)}{8\psi^*},$$

it can be seen that K_{theory} depends linearly on $\Psi_c'''(\phi)$ and nonlinearly on $\Psi_c''(\phi)$. A similar conclusion can be drawn for $R1_{\text{theory}}$ and $R2_{\text{theory}}$ with a closer examination of the expressions. The values of the gains from the theory, simulations, and experiments are plotted against $\Psi_c''(\phi)$ and $\Psi_c'''(\phi)$ in Figure 16.

The analogous plots for the rate expressions are shown in Figure 17. It can be seen from both plots that the gain and rate values obtained from theory, simulations, and experiments share the same trend on their dependence on $\Psi_c''(\phi)$ and $\Psi_c'''(\phi)$. Since the values of the derivatives cannot be obtained without identifying the unstable part of $\Psi_c(\phi)$, it is thus a natural conclusion that the

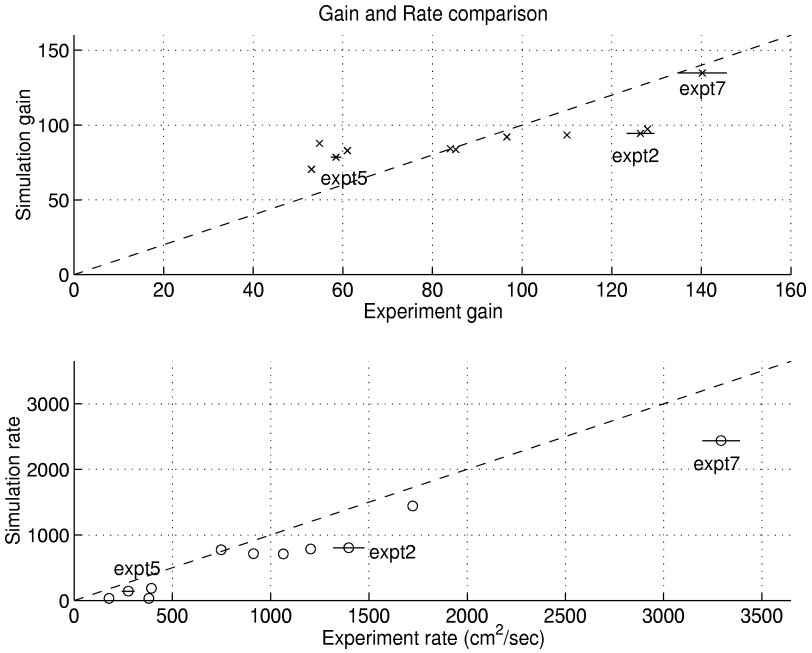

Figure 15: Comparison of gain and rate predicted by simulations and experimental values required for stabilization of stall. The bars in the y direction are error bars associated with the experimentally obtained values.

shape of the unstable part of Ψ_c contains information for the gain and rate requirements of bleed valve control of stall.

A final remark is that the reduction of the bleed actuator requirement via air injection is demonstrated on the Caltech rig for convenience only. Other realizations of compressor characteristic actuation that result in favorable shifting of the characteristic can in principle serve to reduce the actuator requirement as well. Some possible mechanisms include air injection at the tip of the rotor, casing treatments [11], complete or partial guide vanes that redirect the air flow, hub distortion on tip-loaded compressors [17], and mistuning [22]. More information on possible implementations is described in [23].

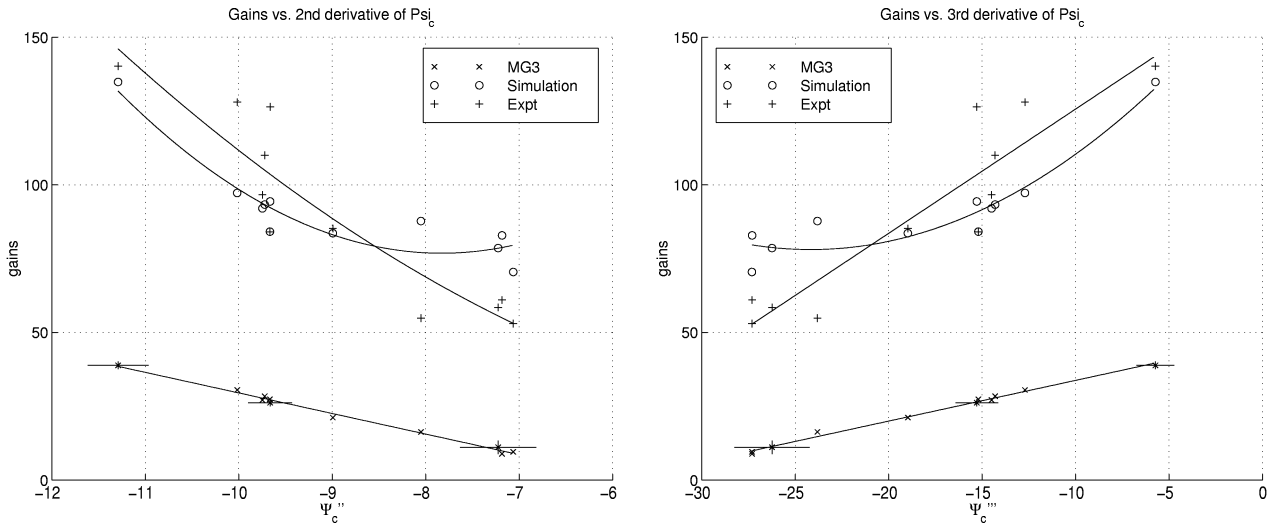

Figure 16: Dependence of K_{theory} on $\Psi_c''(\phi)$ and $\Psi_c'''(\phi)$: experiment (Expt), gain from theory (MG3), and simulation. The error bars in the x direction indicate the error in computing the derivatives (through identifying the unstable of $\Psi_c(\phi)$ using surge cycle data); the error bars in the y direction indicate the error in computing/obtaining the predictions/experimental values.

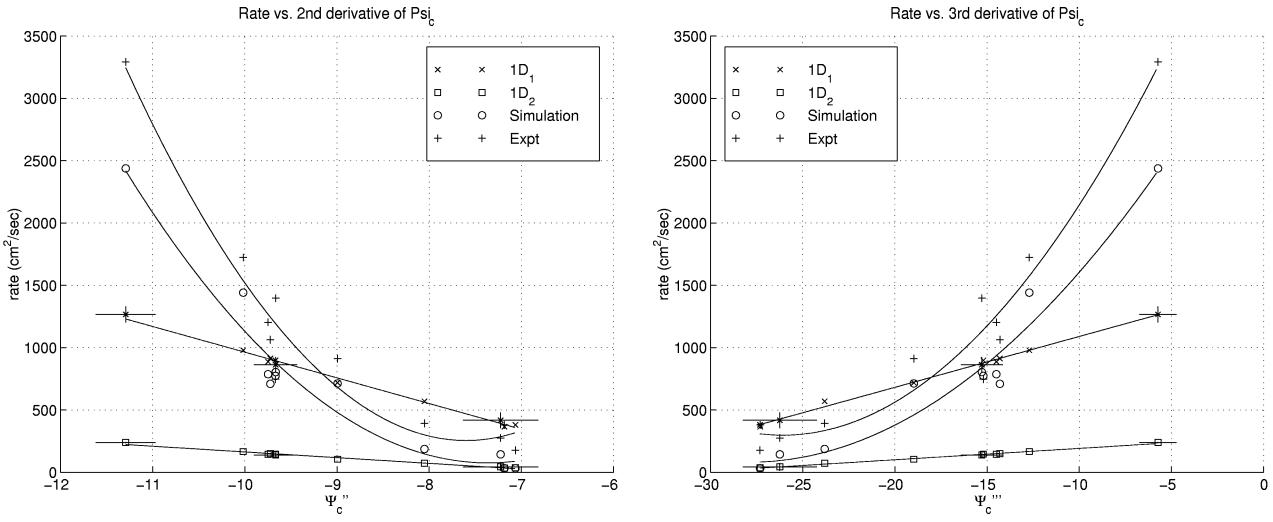

Figure 17: Dependence of R_{theory} expressions on $\Psi_c''(\phi)$ and $\Psi_c'''(\phi)$: experiment (Expt) and rate expression n from theory (ID_n). The error bars in the x direction indicate the error in computing the derivatives (through identifying the unstable of $\Psi_c(\phi)$ using surge cycle data); the error bars in the y direction indicate the error in computing/obtaining the predictions/experimental values.

5 Conclusions and Future Directions

Theoretical and simulation tools have been developed to analyze bleed valve requirements for control of rotating stall and validated against experiments. Compressor characteristic actuation via air injection is found to reduce the bleed valve rate requirement for stall control. *Both* the stable and unstable side of the compressor characteristic are changed by the addition of air injection and found to be crucial in analyzing the closed-loop system.

For the Caltech compression system, the compressor characteristic is more "filled out" on the left of the peak in the presence of air injection, and the peak location, second, and third derivative at the peak are different than those of the unactuated characteristic. This change of system characteristics reduces the bandwidth and magnitude requirements of a bleed actuator in performing bleed valve controls of rotating stall. With a compressor rotor frequency of 100 Hz, active control of stall with a high speed bleed valve is achieved *only when the compressor characteristic is actuated.* Furthermore, the experiments show that the bleed valve rate requirement is reduced from approximately 3300 cm^2/sec to below 230 cm^2/sec when the amount of compressor characteristic actuation is increased. This actuation is captured by a change of the shape and a shift in the peak of the compressor characteristic. Theoretical tools based on a low order model (2-3 states) and simulations based on a reduced order distributed model (37 states) have been developed to estimate the gain and rate requirements of the bleed controller. All of the proposed analytical formulas and simulations share the same qualitative trends with respect to Ψ_c'', Ψ_c''', and the experiment. The agreement implies that bleed valve control of rotating stall depends crucially on the rate limit of the bleed valve which in turn depends on *both* the stable and the *unstable* part of the compressor characteristic.

The effects of air injection are accounted for via a shift of the compressor characteristic in this paper, whereas the actual effects are much more sophisticated. A more detailed fluid dynamic model of the effects of air injection on compressors will provide a more accurate basis for theoretical analysis as well as simulations.

Aside from rate limit, bandwidth and delay are also parts of actuator dynamics. A comparison study between the theory, simulation, and experiments on various features of actuator limitations will not only validate the model and the analysis, but also allow a more complete picture of how control implementation is affected. The resulting sensitivity analysis can be used as a design guide line for compressor-bleed pair construction with intent of active control of stall implementations.

Acknowledgment

The authors would like to thank United Technologies Research Center (UTRC) for loan of the high speed bleed valve that was used to achieve the results reported in this paper.

References

[1] O. O. Badmus, S. Chowdhury, K. M. Eveker, and C. N. Nett. Simplified Approach for Control of Rotating Stall 1 and 2. *ASME Journal for Propulsion and Power*, 11(6):1195–1223, 1995.

[2] O. O. Badmus, S. Chowdhury, and C. N. Nett. Nonlinear Control of Surge in Axial-Compression Systems. *Automatica*, 32(1):59–70, 1996.

[3] R. L. Behnken. Nonlinear Control and Modeling of Rotating Stall in an Axial Flow Compressor, September 1996. Ph.D thesis, California Institute of Technology.

[4] R. L. Behnken, M. Leung, and R. M. Murray. Characterizing the Effects of Air Injection on Compressor Performance for use in Active Control of Rotating Stall. In *Proceedings of The International Gas Turbine and Aeroengine Congress and Exhibition*, 1997. ASME 97-GT-316.

[5] R. D'Andrea, R.L. Behnken, and R.M. Murray. Active Control of an Axial Flow Compressor via Pulsed Air Injection. *ASME Journal of Turbomachinery*, 119(4):742–752, 1998.

[6] I.J. Day. Active Suppression of Rotating Stall and Surge in Axial Compressors. *ASME Journal of Turbomachinery*, 115:40–47, 1993.

[7] Allison Engines. Advanced Control for Air Breathing Engines - Volume 3, Allison Gas Turbine, July 1993. N94-12272, U.S. Department of Commerce, National Technical Information Service.

[8] General Electric Aircraft Engines. Advanced Control for Air Breathing Engines - Volume 2, General Electric Aircraft Engines, July 1993. N94-12271, U.S. Department of Commerce, National Technical Information Service.

[9] K.M. Eveker, D.L. Gysling, and C.N. Nett. Integrated Control of Rotating Stall and Surge in Aeroengines. In *Proceedings of The Internation Society for Optical Engineering*, pages 21–35, April 1995.

[10] C. Freeman, A. G. Wilson, I. J. Day, and M. A. Swinbanks. Experiments in Active Control of Stall on an Aeroengine Gas Turbine. In *International Gas Turbine and Aeroengine Congress and Exhibition*, 1997. ASME 97-GT-280.

[11] E.M. Greitzer. Review - Axial Compressor Stall Phenomena. *ASME Journal of Fluids Engineering*, 102:134–151, 1980.

[12] E.M. Greitzer and F.K. Moore. A Theory of Post-Stall Transients in Axial Compression Systems: Part 1–Development of Equations, Part 2–Application. *ASME Journal for Engineering for Power*, 108:68–78, 231–239, 1986.

[13] D.L. Gysling and E.M. Greitzer. Dynamic Control of Rotating Stall in Axial-flow Compressors using Aeromechanical Feedback. *Journal of Turbomachinery*, 117(3):307–319, 1995.

[14] J. M. Haynes, G. J. Hendricks, and A. H. Epstein. Active Stabilization of Rotating Stall in a Three-Stage Axial Compressor. *Journal of Turbomachinery*, 116:226–239, 1994.

[15] United Technologies Incorporated. Advanced Control for Air Breathing Engines - Volume 1, Pratt and Whitney, July 1993. N94-12270, U.S. Department of Commerce, National Technical Information Service.

[16] D. C. Liaw and E. H. Abed. Control of Compressor Stall Inception—A Bifurcation-theoretic Approach. *Automatica*, 32(1):109–115, 1996.

[17] J.G. Lucas, H.B. Finger, and R.E. Filippi. Effect of Inlet-Annulus Area Blockage on Overall Performance and Stall Characteristics of an Experimental 15-Stage Axial-Flow Compressor. Technical Report R&M E53L28, NACA, 1958.

[18] C. A. Mansoux, D. L. Gysling, J. D. Setiawan, and J. D. Paduano. Distributed Nonlinear Modeling and Stability Analysis of Axial Compressor Stall and Surge. In *American Control Conference*, pages 2305–2316, 1994.

[19] R.M. Murray, E.L. Wemhoff, and Michael Kantner. *Sparrow Reference Manual.* California Institute of Technology, February 1995.

[20] J.D. Paduano, A.H. Epstein, L. Valavani, J.P. Longley, E.M. Greitzer, and G.R. Guenette. Active Control of Rotating Stall in a Low-Speed Axial Compressor. *ASME Journal of Turbomachinery*, 115:48–56, 1993.

[21] Y. Wang and R. M. Murray. Effects of Noise, Magnitude Saturation and Rate Limits on Rotating Stall Control. In *Proceedings of Conference on Decision and Control*, pages 4682–4689, 1997.

[22] D. S. Whitehead. Torsional Flutter of Unstalled Cascade Blades at Zero Deflection. *Great Britain A.R.C.*, RM 3429, 1964.

[23] S. Yeung and R. M. Murray. Actuator Bandwidth and Rate Limit Reduction for Control of Compressor Rotating Stall. U. S. Patent Application, Serial No. 60/037,774, October, 1997.

[24] S. Yeung and R. M. Murray. Nonlinear Control of Rotating Stall using 1-D Bleed Valve with Continuous Air Injection. In *Proceedings of Joint Propulsion Conference and Exhibit*, Seattle Washington, 1997. AIAA 97-2660.

[25] S. Yeung and R. M. Murray. Reduction of Bleed Valve Rate Requirements for Control of Rotating Stall using Continuous Air Injection. In *Proceedings of Conference on Control Applications*, pages 683–690, 1997.